Environ. Eng. Res. 2023; 28(3): 220074
https://doi.org/10.4491/eer.2022.074

pISSN 1226-1025
eISSN 2005-968X

Research

Tuning the structural, magnetic, and optical properties of $ZnO/NiFe_2O_4$ heterojunction photocatalyst for simultaneous photodegradation of Rhodamine B and Methylene Blue under natural sunlight

Yeni Stiadi, Tio Putra Wendari, Zilfa, Zulhadjri, and Rahmayeni†

Department of Chemistry, Faculty of Mathematics and Natural Sciences, Universitas Andalas, Kampus Limau Manis, Padang 25163, Indonesia

Received February 14, 2022 **Revised** April 23, 2022 **Accepted** May 04, 2022

ABSTRACT

The magnetic nanocomposites of $ZnO/NiFe_2O_4$ were synthesized using a hydrothermal method in organic solvent-free media for application as a heterojunction photocatalyst. XRD measurements confirmed the formation of the required phases of nanocomposites with no impurity phases observed. The SEM and TEM analysis confirmed the morphology and shape of composite as being spherical and square-like grain. The magnetic properties of composites measured using vibrating sampler magnetometer (VSM) under an applied field of ±2 T showed a soft ferromagnetism. Band gap energy of the $ZnO/NiFe_2O_4$ sample was found to be lower than the pure ZnO nanoparticles. The photocatalytic activity of samples was evaluated by monitoring the simultaneous degradation of the mixed dye model of Rhodamine B and Methylene Blue under visible-light irradiation. Compared with pure ZnO, the nanocomposites exhibited a better photocatalytic performance with a degradation percentage of 98% for Rhodamine B and 97% for Methylene Blue in mix solution after 3 h of irradiation.

Keywords: Heterojunction photocatalyst, Methylene blue, Rhodamine B, Simultaneous degradation, $ZnO/NiFe_2O_4$

Graphical Abstract

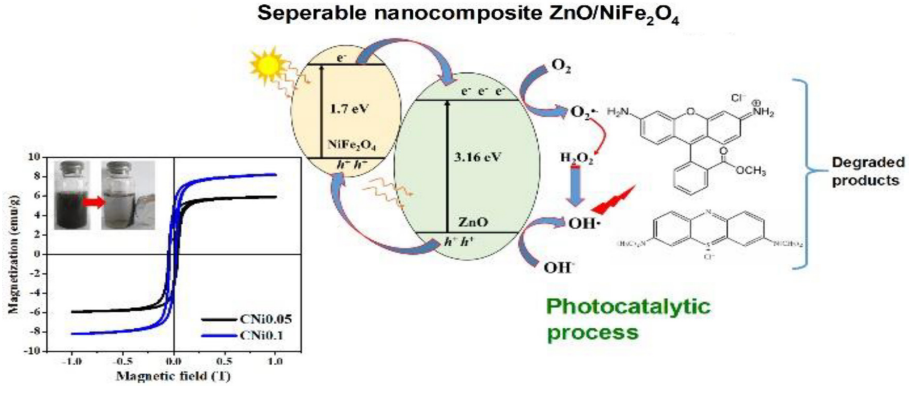

† Corresponding author
E-mail: rahmayenni@sci.unand.ac.id
Tel: +6281363100506
Fax:
ORCID: 0000-0003-2569-9914

1. Introduction

Environmental degradation is a common outcome of unregulated industrial development. Certain industrial facilities would discharge organic compounds into the environment in the form of dyes and oily liquids [1]. The textile and dyeing industries make use of large amounts of water and are among the most water-consuming industries in existence. About 10-20% of the unfixed dyes like Rhodamine B, Victoria Blue, Rose Bengal, Indigo Red, Caramine, Red 120, Eriochrome, Methylene Blue (MB), Black-T (EBT), Thymol Blue, Methyl Red, Methyl Orange, Malachite Green, and Direct Blue 71 are lost in the process water during the dyeing operation, which comes out as a colored effluent from the facility and is released into the environment [2,3]. Most dyes are toxic and carcinogenic because they contain the azo group (N=N), which can cause various harmful diseases when accumulated in the body. Its stable structure makes it difficult to be biodegraded by microorganisms [4–6]. Rhodamine B and Methylene Blue are toxic organic dyes containing azo groups that dissolve easily in water and can irritate the respiratory system, skin, and eyes. Hence, removing these dyes from wastewater is a priority [7].

Several methods have been developed to remove organic dye pollution from water, such as reverse osmosis, coagulation, precipitation, deposition, gravity and flotation, electrochemical technique, photodegradation and adsorption [8–10]. Recently, the removal of organic pollutants at ambient conditions employing semiconductors as photocatalyst has attracted attention because it is an emerging green method. Semiconductor-based photocatalysts can absorb photons to generate electron–hole pairs that can drive the oxidation or reduction of organic compounds, breaking them down into simple molecules, i.e., H_2O and CO_2 [11]. In addition, the use of this method for handling dye waste does not produce new waste. Photocatalysis has been applied for the disinfection and detoxification of effluents of various industries [12].

Several researchers have used the photocatalysis method to process waste dye using different semiconductors. T. Le Thi Thanh et al. used C/Fe Co-Doped titanium dioxide coated on activated carbon for the photocatalytic degradation of Rhodamine B [13]. V.F. Marañon-ruiz et al. used ZrO_2-doped TiO_2 as catalyst to investigate methyl orange and Rhodamine B through mineralization studies. ZrO_2-doped TiO_2 composites exhibited a higher photocatalytic activity than just utilizing the synthesized TiO_2 and a commercial P25 [14]. Gelatin/CuS/PVA nanocomposites have been used for Rhodamine B dye photocatalytic degradation under solar light. RhB photocatalytic degradation in aqueous gelatin/CuS/PVA nanocomposite was found to follow a pseudo-first-order kinetics [7]. Iron titanate (Fe_2TiO_5) nanoparticles with an orthorhombic structure were successfully used as photocatalyst for the degradation of Methylene blue under natural sunlight [15].

ZnO is a semiconductor that has recently been attracting attention due to its interesting properties and wide applications. As a photocatalyst, the wide bandgap (3.2 - 3.4 eV) of ZnO allows it to absorb UV light for the required bandgap excitation, charge carrier generation, while absorbing less in the visible spectrum [16]. In addition, ZnO can undergo photocorrosion if used alone in the photocatalytic process. To increase the ability of ZnO to absorb well in the visible spectrum and reduce photocorrosion, it has been doped with various materials, among them is the ferrite compound MFe_2O_4 [17,18]. Much effort has been expended to extend the photoresponse of ZnO into the visible region. One promising way is coupling two different semiconductors to form a *p*-*n* heterojunction. ZnO is an *n*-type semiconductor; it can be combined with a *p*-type semiconductor such as MFe_2O_4 to form a *p*-*n* heterojunction structure [19,20]. This combination could more effectively inhibit the recombination of the photogenerated electron–hole pairs to enhance the material's photocatalytic activity. The combination of ZnO and MFe_2O_4 to form ZnO/MFe_2O_4 composite can absorb both in the UV spectrum and in the visible spectrum while exhibiting magnetism. For heterogeneous catalysis, magnetism is highly desired because it allows the catalyst particle to be easily collected out of the solution using an external magnetic field [21–23].

Various ferrites have been used to synthesize ZnO/MFe_2O_4 composites, including $NiFe_2O_4$, $ZnFe_2O_4$, $CaFe_2O_4$, $CoFe_2O_4$, Fe_3O_4, and $MnFe_2O_4$ [24–29]. Among these ferrite materials, $NiFe_2O_4$ is particularly attractive due to its moderate magnetic properties, good catalytic properties, and chemical stability [30]. If $NiFe_2O_4$ is combined with ZnO, the resulting composite would have better absorption in the visible spectrum while resisting photocorrosion. ZnO/$NiFe_2O_4$ composites have been synthesized using various methods such as hydrothermal, solvothermal, solid-state, co-precipitation, and wet chemical methods; They have also been applied in multiple domains, as a photocatalyst and as an adsorbent in the handling the organic compounds in wastewater to name a few [31,32]. However, the use of these composites as photocatalysts has not been reported for the simultaneous degradation of Rhodamine B and Methylene Blue dyes in aqueous solutions. Simultaneous characterization of the degradation behavior of multiple dyes is an attempt to mimic the real world condition in which dye pollutants often exist [33].

In this study, ZnO/$NiFe_2O_4$ nanocomposites were synthesized via the simple hydrothermal method in organic solvent-free media. The structure, morphology, magnetic, and optical properties of the composites were investigated in detail. The synthesis method and photocatalytic performance of ZnO/$NiFe_2O_4$ investigated by simultaneous degradation of Rhodamine B and Methylene Blue under natural sunlight irradiation has been not reported yet in the literature. The effects of various operating conditions were also investigated, namely concentration of dyes, irradiation time, and catalyst loading.

2. Experimental Section

2.1. Materials

This study made use of $Zn(NO_3)_2.4H_2O$, $Ni(NO_3)_2.4H_2O$, NaOH, Fe $(NO_3)_3$.$9H_2O$, which were purchased from Merck. Rhodamine-B, Methylene Blue, distilled water, and universal pH paper were also used.

2.2. Synthesis of $NiFe_2O_4$ Particles

$NiFe_2O_4$ particles were synthesized with the following procedure [34]. $Ni(NO_3)_2.6H_2O$ and $Fe(NO_3)_3.9H_2O$ (mole ratio of Ni^{2+}: Fe^{3+}

= 1: 2) was dissolved in 100 mL of distilled water. The mixture was stirred until a homogeneous brown solution was obtained. NaOH solution was added dropwise to the mixture under stirring until it was at pH 12. The mixture was transferred into an autoclave and heated for 3 h at 180 °C. The $NiFe_2O_4$ powder produced was filtered and washed with distilled water until neutral, then dried at 100 °C for 2 h. A sample of the $NiFe_2O_4$ nanoparticle was sent for characterization. The final product of $NiFe_2O_4$ nanoparticle was used for the synthesis of $ZnO/NiFe_2O_4$ nanocomposite.

2.3. Synthesis of $ZnO/NiFe_2O_4$ Nanocomposites.

$ZnO/NiFe_2O_4$ nanocomposite was synthesized via the hydrothermal method, as reported earlier [34]. $Zn(NO_3)_2.4H_2O$ and $NiFe_2O_4$ nanoparticles (obtained from the procedure in Section 2.2) with various mole ratios of Zn^{2+} to $NiFe_2O_4$ (1: 0.05, and 1: 0.1) were mixed into 40 mL distilled water and stirred for 1 h. 2 M NaOH solution was added dropwise to the mixture under continuous stirring until it reached pH 12. The mixture was heated for 3 h at 180 °C. The precipitate was filtered and washed with distilled water until neutral, then dried at 100 °C for 2 h. The $ZnO/NiFe_2O_4$ nanocomposites obtained were labelled as CNi0.05 and CNi0.1 for the mole ratios of 1: 0.05 and 1: 0.1, respectively.

2.4. Characterization

The crystalline phases in the products were analyzed by X-ray diffraction (XRD; XPERT-PRO). The crystal structure was refined by the Le Bail refinement technique using the RIETICA program [31]. Scanning Electron Microscopy-Energy Dispersive X-ray (SEM-EDX; FEI Inspect S50) was used to examine grain size and morphology. Magnetization as a function of an applied field was measured using Vibrating Sampler Magnetometer (VSM; OXFORD 1.2H). Meanwhile, UV-Visible Diffuse Reflectance Spectrophotometer (UV-Vis DRS; Shimadzu 2450) was used to determine optical properties. The absorbance of dyes before and after the photocatalytic process was obtained using a UV-Vis spectrophotometer (Spectronic 20).

2.5. Photocatalytic Activity Test

The photocatalytic activity of as-prepared samples was assayed by modifying the previous method [32]. First, stock solutions of Rhodamine B and Methylene Blue (1000 mg L^{-1}) were prepared and then diluted to various concentrations (7.5, 10, 12.5, and 15 mg L^{-1} for Rodamine B and 10, 20, 30, and 40 mg L^{-1} Methylene Blue. 0.02 g of photocatalyst was added to 20 ml of Rhodamine B solution and Methylene Blue for optimal catalytic performance. The suspensions were irradiated under natural sunlight for 3 h (11.00 AM - 01.00 PM). The volume of liquid that evaporated during irradiation by sunlight was replaced by adding distilled water. The amount of water added to the bath was determined by weighing the bath containing the catalyst and dye before and after being exposed to sunlight. After that, the solution was separated from the catalyst. The absorbance of the solution was measured at 553 nm for Rhodamine B and 655 nm for Methylene Blue to determine the concentration of degraded dyes. The catalyst activity was tested against dye degradation simultaneously by varying the volume of Rhodamine B and Methylene Blue solutions, as shown in Table S1. Several parameters related to the photocatalytic test, such as concentration, duration of exposure, type of catalyst, and catalyst loading, were also investigated.

3. Results and Discussion

3.1. Characterization

Fig. 1 shows the XRD pattern of the composites CNi0.05 and CNi0.1 samples synthesized via the hydrothermal method. The XRD patterns were indexed according to the standard diffraction pattern of ZnO with the hexagonal *P*63*mc* space group (ICSD-155780) and $NiFe_2O_4$ with the cubic *Fd*-3*ms* space group (ICSD-153013). Both nanocomposite samples exhibited the dominant diffraction peaks at $2\theta = 31.7^o$, 34.4^o, and 36.2^o with the miller indices of (100), (002), and (101), corresponding to ZnO nanoparticles in the composite. $NiFe_2O_4$ specific peaks at $2\theta = 35.7^o$ with 311 miller index as denoted by the asterisk (*) symbol were also observed in both samples, indicating the existence of this phase in the composite samples. The presence of typical XRD peaks of ZnO and $NiFe_2O_4$ phases without any additional peaks demonstrated that the single-phase $ZnO/NiFe_2O_4$ nanocomposite was successfully formed using this method. The presence of both phases and their crystal structure was further confirmed by the refinement analysis discussed below.

Le Bail refinement of the XRD data was conducted to study the phase formations and crystal structure in detail. Considering the existence of both ZnO and $NiFe_2O_4$ phases, the XRD data was refined using the multiphase refinement system [37]. Refinement was carried out using ZnO as the major phase and $NiFe_2O_4$ as the secondary phase. The structural parameters of ZnO phase with *P*63*mc* space group ($a = b = 3.2503$ Å, $c = 5.207$ Å, $a = b = 90°$, $g = 120°$) (ICSD-157724) and $NiFe_2O_4$ phase with *Fd*-3*ms* space group ($a = b = c = 8.4211$ Å, $a = b = g = 90°$) (ICSD-158834) were used as the initial parameter.

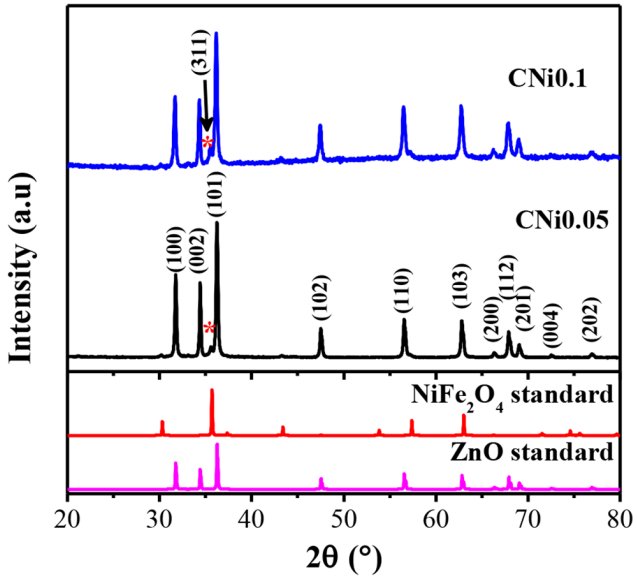

Fig. 1. The XRD pattern of CNi0.05 and CNi0.1 composite samples.

Table 1. Refined Cell Parameters of CNi0.05 and CNi0.1 Samples

Parameter	CNi0.05		CNi0.1	
Phase	ZnO	$NiFe_2O_4$	ZnO	$NiFe_2O_4$
Space group	*P*63*mc*	*Fd*-3*ms*	*P*63*mc*	*Fd*-3*ms*
Crystal class	Hexagonal	Cubic	Hexagonal	Cubic
a (Å)	3.2488(5)	8.3407(1)	3.2526(8)	8.3837(6)
b (Å)	3.2488(5)	8.3407(1)	3.2526(8)	8.3837(6)
c (Å)	5.1984(1)	8.3407(1)	5.2072(2)	8.3837(6)
V(Å^3)	47.518(4)	580.242(3)	47.711(2)	589.273(4)
Z	2	8	2	8

The profile of refinement plots of CNi0.05 and CNi0.1 samples is displayed in Fig. S1. The plots show a good fit between the experimental and calculated patterns, with all diffraction peaks fitting with the Bragg reflection. Moreover, the small peaks of the $NiFe_2O_4$ phase observed at 2q = 35.7° (highlight in Fig. 1) in the composite samples can be indexed with the Bragg reflection of the cubic $NiFe_2O_4$ as shown in the inset of Fig. S1. The results confirmed that the $NiFe_2O_4$ phases were composited with ZnO phases. Further detailed parameters of the ZnO/$NiFe_2O_4$ composite sample obtained from XRD data are given in Table 1. The ZnO phase was found to adopt a hexagonal structure corresponding to the space group *P*63*mc*, while the $NiFe_2O_4$ phase adopted a cubic structure corresponding to the *Fd*-3*ms* space group.

The grain size and morphology of the composites were analyzed using SEM, as shown in Fig. 2. The SEM micrograph of the CNi0.05 sample (Fig. 2a) shows a spherical and square-like grain morphology with an average length of 150 nm, average width of 120 nm, and average thickness of 85 nm, which are typical features of ferrite compounds. Moreover, both the morphology and size were significantly influenced by the amount of $NiFe_2O_4$. As the amount of $NiFe_2O_4$ increased in CNi0.1 composites (Fig. 2b), the average plate-like grain size increased to 200 nm long, 175 nm wide, and 85 nm thick. The shape and size of the particles were comparable to those obtained by previous researchers who used the sol-gel method in the synthesis of ZnO/$NiFe_2O_4$ composites [38]. It was also observed that the CNi0.05 sample had a more uniform grain shape compared to the CNi0.1 sample. The small and homogeneous particle shape was very beneficial for its application as a photocatalyst because it provides a larger contact area between the catalyst and the substrate [39].

The elemental composition of the composite samples was analyzed using EDX. The EDX spectra of CNi0.05 (Fig. 3c) and CNi0.1 (Fig. 2d) indicated the presence of Zn, Fe, Ni, and O. From the peak intensity of the EDX spectrum, CNi0.1 exhibited a higher intensity of Ni and Fe peaks compared to CNi0.05 due to the higher content of $NiFe_2O_4$ in the composite. A more detailed analysis of the particle shape can be seen from the TEM results (Fig. 2e). The TEM image revealed that the $NiFe_2O_4$ nanoparticles (black region) were coated with ZnO (white region), forming a core and shell structure. This structure facilitated electron transfer in composite (between $NiFe_2O_4$ and ZnO), thereby potentially facilitating the photocatalytic process [21,40].

The magnetic properties of composite samples were analyzed using VSM at room temperature as shown in Fig. 3. The pristine ZnO was reported to be diamagnetic, which means it did not have

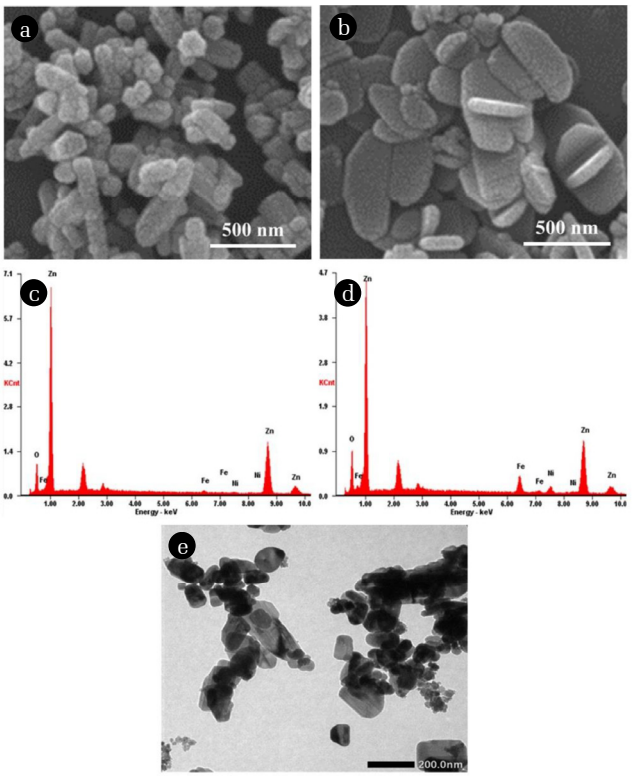

Fig. 2. SEM-EDX analysis of (a,c) CNi0.05 and (b,d) CNi0.1 and (e) TEM image of CNi0.05.

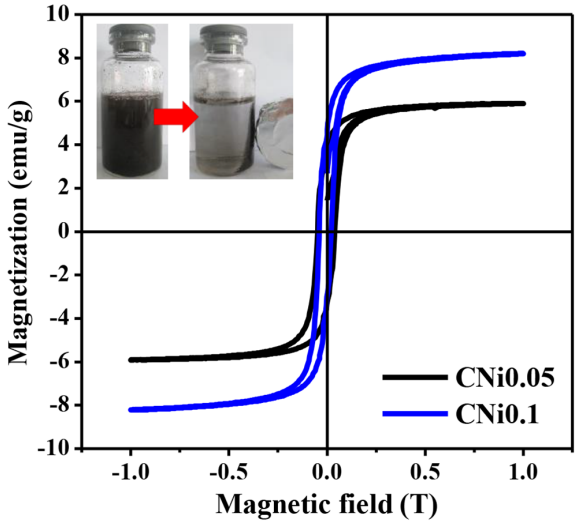

Fig. 3. Magnetization versus applied magnetic field curve (*M* – *H*) of CNi0.05 and CNi0.1 measured at room temperature.

a permanent dipole in its structure. The hysteresis curves indicated that both composite samples have soft ferromagnetic behavior. The CNi0.05 sample exhibited a typical ferromagnetic *M-H* loop, with the remnant magnetization (M_r) of 3.5 emu/g and coercive field (H_c) of 228 Oe. It is observed that the increase in $NiFe_2O_4$ amount in the CNi0.1 sample resulted in a stronger ferromagnetism. The

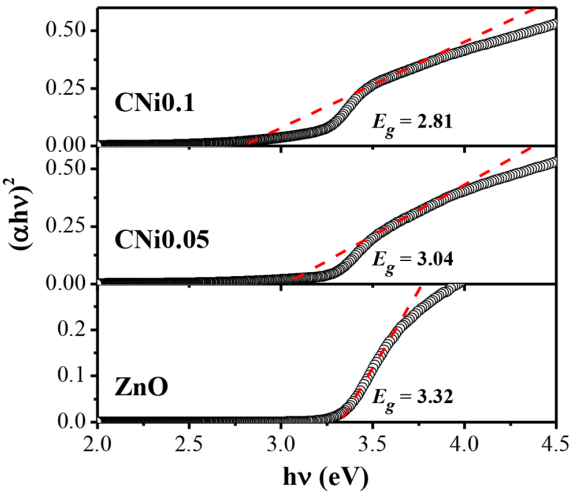

Fig. 4. Tauc's plots of ZnO, CNi0.05, and CNi0.1 samples for the determination of optical bandgap energy (E_g)

M_r and H_c of the CNi0.1 sample were about 4.2 emu/g and 392 Oe, respectively. The magnetization of the samples could also be affected by the raised structure effects due to the redistribution of cations in the spinel structure of $NiFe_2O_4$ core or the diffusion of Zn ions into the spinel structure [21]. Magnetism is an attractive property to have as a photocatalyst, since it allows for easy separation between the solid catalyst particle and the reaction medium [19].

The optical properties of the composite samples were assessed by measuring its bandgap energy (E_g) via DRS UV-Vis analysis. E_g was fitted according to Tauc's method from plots of $(\alpha h\upsilon)^n$ versus $h\upsilon$, where n = 1/2 denotes the indirect bandgap and n = 2 denotes the direct bandgap. As a result, the curves of all samples were well described by Tauc's plots with n = 2 shown in Fig. 4, which contains the linear extrapolation that suggests the presence of a direct bandgap transition behavior [25]. The line fit yields an estimated E_g value of approximately 3.32 eV for pristine ZnO. The value gradually decreased with increasing $NiFe_2O_4$ content in composite samples, measuring in at 3.04 for CNi0.05 and 2.81 for CNi0.1. It can be concluded that increasing the amount of $NiFe_2O_4$ in the composite effectively decreases the E_g of the synthesized composite. The decrease in the bandgap of pristine ZnO (3.32 eV) is due to the expansion of the conduction and valence bands of ZnO. It may also be attributed to the interaction of the atoms of $NiFe_2O_4$ in the ZnO structure. The reduction in E_g is advantageous in its application as a photocatalyst because it can absorb well in the visible spectrum [41]. We suggest that the formation of heterojunction in ZnO-semiconductor interface can enhance charge separation of photo-generated e^-/h^+ pairs and improve the photocatalytic efficiency in the visible spectrum.

3.2. Photocatalytic Properties Assay

The effect of composite type on the degradation of Rhodamine B and Methylene Blue dyes was determined simultaneously by varying the irradiation time to 1 h, 2 h, and 3 h under sunlight. The dye volume was set at 20 mL with an initial concentration of 10 mg L^{-1} and a catalyst loading of 0.02 g, as shown in Fig. 5. The determine the extent of dye degradation, the absorptivity of the medium was measured using a UV-vis spectrophotometer. By using the following equation

$$D\ (\%) = A_0\text{-}A_t/A_0 \times 100\%$$

where A_0 is the initial concentration and A_t is the concentration at time t, then D is the amount of degraded dye obtained. When the nanocomposites were the catalyst, the degradation percentage of Rhodamine B and Methylene Blue dyes was higher compared to ZnO and without catalyst. Such result indicates that the photocatalytic activity of Rhodamine B and Methylene Blue degradation was effectively enhanced by the presence of nanocomposite catalyst. Without a catalyst, the degradation percentage for Rhodamine B only reached 10% and the degradation percentage of methylene blue reached 30% after 3 h. The dyes degrade even without a catalyst because the chromophore group of the dye absorbs photons. The absorbed energy breaks the bonds in the chromophore region in the dye, disintegrating it into smaller molecules which in turn break down further into simple compounds [7,25]. The higher degradation percentage of the dye in composite samples was because the composites have a smaller bandgap than ZnO (3.32 eV). Therefore, they absorb light more efficiently in the visible spectrum. ZnO is more active in the UV spectrum but is less absorptive in visible light. As a result, the formation of hydroxyl radicals ($^{\bullet}OH$) was responsible for the degradation process, but it was inhibited.

The highest percentage of degradation was achieved using the CNi0.05 composite as a catalyst for both dyes. The degradation percentage reached 98% for Rhodamine B and 97% for Methylene Blue after irradiation for 3 h under natural sunlight. Without light, the degradation percentage of CNi0.05 composite only reached 6-8% after 3 h. These results proved that the degradation of dye by CNi0.05 occurred through the photocatalysis since the irradiation process significantly increased the percentage of degradation. It is suggested that the CNi0.05 composites have a smaller and more homogeneous grains than the CNi0.1 composite. This smaller particle size of the CNi0.05 composite increased the number of active sites on the catalyst that could react with the dye molecules, resulting in increased photocatalytic activity, as observed in the SEM and TEM micrographs. Besides, increasing the amount of ferrite increased the magnetic properties of the composite (Fig. 3). The higher magnetic properties of the CNi0.1 composite also affected the photocatalysis since the particles tend to agglomerate. This phenomenon possibly reduced the number of available active sites on the catalyst to interact with the dye, hence lowering the activity.

The effect of catalyst loading on photocatalysis is economically significant [37]. The experiment was carried out in the following conditions: the volume of the dye solution was 20 mL, the catalyst loading ranged among 0.005 g, 0.010 g, 0.015 g, and 0.020 g, 3 h of exposure time, and the composite used was CNi0.05. Fig. 6a shows the degradation percentage of Rhodamine B and Methylene Blue using a CNi0.05 catalyst at varying loading. It was observed that the degradation percentage increased with the increasing catalyst loading. The increase was due to the increase in the number of $^{\bullet}OH$ radicals generated. $^{\bullet}OH$ radicals are responsible for the degradation of dyes in photocatalysis [38]. The degra-

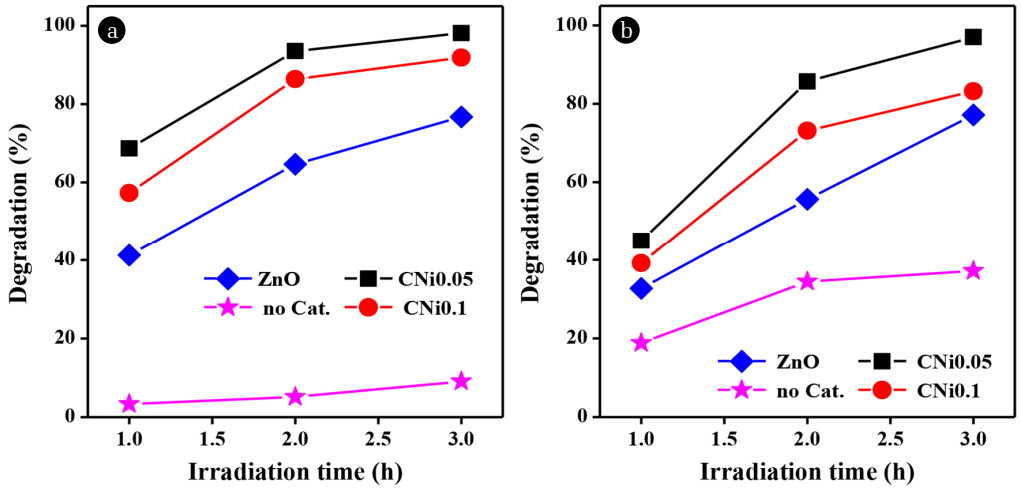

Fig. 5. Effect of irradiation time on the degradation percentage of (a) Rhodamine B and (b) Methylene Blue in mixed solution using different catalysts.

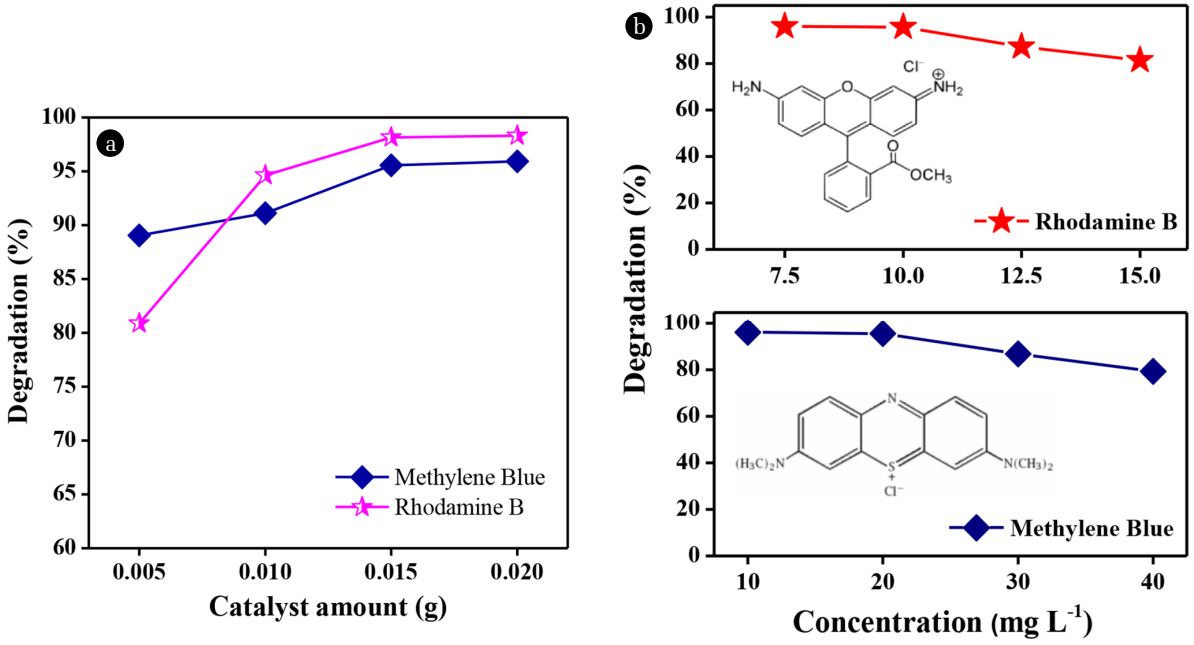

Fig. 6. The degradation percentage of Rhodamine B and Methylene Blue dyes in contact with CNi0.05 composite at (a) various catalyst loading (b) various dye concentration

dation percentages of Rhodamine B and Methylene Blue solutions using 0.015 g of catalyst reached 98.2% and 95.6%, respectively. Increasing the amount of catalysts did not significantly impact the increase in the percentage of dye degradation. Therefore, 0.015 g is more efficient for further work from an economic point of view.

The effect of concentration on the degradation percentage of the dye was investigated by varying the concentration of the 20 mL of Rhodamine B solution [7.5, 10, 12.5, and 15 mg L^{-1}]. 0.015 g of CNi0.05 catalyst was added and stirred evenly. Next, the mixture was exposed to the natural sunlight for 3 h. The same procedure was conducted for Methylene Blue at various concentrations (10, 20, 30, and 40 mgL^{-1}). Fig. 6b shows the effect of concentration on the degradation percentage of Rhodamine B and Methylene Blue dyes using the CNi0.05 composite as a catalyst. The higher the dye concentration, the lower the degradation percentage because the number of dye molecules increases in the liquid. A large number of dye molecules in the liquid can inhibit light penetration towards the catalyst, which prevented the formation of $^{\bullet}OH$ radicals. The optimum condition was achieved at the concentration of 10 mg L^{-1} for Rhodamine B and 20 mg L^{-1} for Methylene Blue with the percentage of degradation reaching 95.7% and 95.5%, respectively.

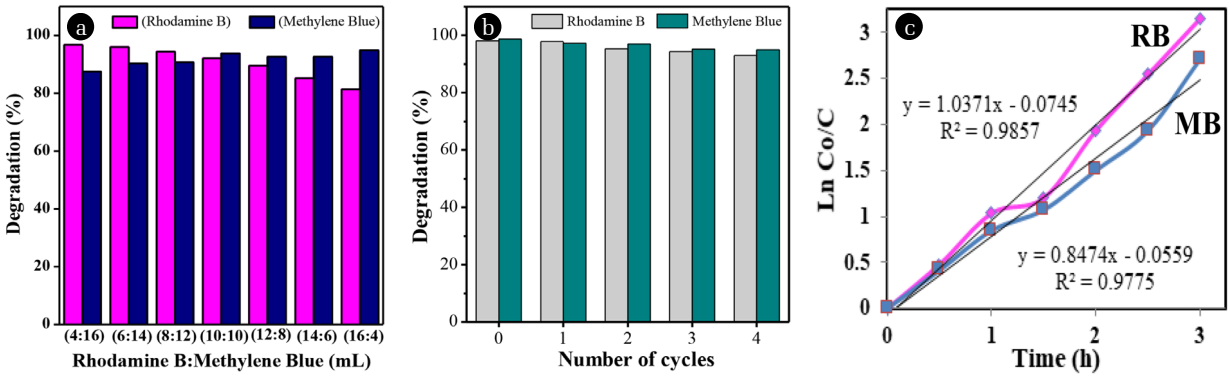

Fig. 7. (a) The simultaneous degradation of mixed Rhodamine B and Methylene Blue at different volumetric ratios and (b) Reusability test of CNi0.05 composite as the catalyst. (c) Plot of ln C_o/C vs time illustrates the reaction kinetics of degradation

The difference in the optimal concentration was due to the differences in the molecular structure of each dye. The higher degradation of Methylene Blue even at higher concentration was due to its simpler structure, bearing an azo group which is easier to break in photocatalysis (Inset of Fig. 6b) [39].

The simultaneous degradation process was evaluated by mixing the optimal concentration of Rhodamine B (10 mg L^{-1}) and Methylene Blue (20 mg L^{-1}) solutions at various volume ratios (Table S1). From various comparisons of Rhodamine B and Methylene Blue concentrations, the optimum condition was achieved at a volumetric ratio of 1:1 as shown in Fig. 7a. In this comparison, the degradation percentage of Rhodamine B and Methylene Blue was almost the same. These results indicated that CNi0.05 composites can be used to degrade dyes simultaneously so that they have the potential to be used as a catalyst to degrade the dye wastes or other organic pollutants.

A reusability test was performed to assess the nanocomposite's retention of catalytic activity over multiple rounds of dye degradation reaction. A dye mixture with an optimal volumetric ratio of 1:1 was used in this test. The CNi0.05 loading was set at 0.015 g, while the total volume of the dye mixture was 20 mL (10 mL of Rhodamine B 10 mg L^{-1} and 10 mL Methylene Blue 20 mg L^{-1}). In each cycle, the reaction medium was irradiated for 2 h. As a heterogeneous and magnetic catalyst, the ZnO/$NiFe_2O_4$ composite can be separated from the reaction solution by an external magnet and transferred to a fresh reaction medium to start the next cycle. The results of the reusability test are shown in Fig. 7b. The CNi0.05 samples retained good activity in the degradation of both Rhodamine B and Methylene Blue dyes. The degradation yield hovered above ~95% after 5 reaction cycles. The reduced degradation activity seemed to result from the washing and magnetic separation step to reuse the heterogeneous catalyst and the chemisorption or physical process due to blocking of surface sites. Therefore, the CNi0.05 composite was deemed to have good physicochemical stability as a heterogeneous catalyst in the photocatalytic processes through several cycles of reuse.

The reaction kinetics of the photodegradation of Rhodamine B and Methylene Blue dyes using a ZnO/$NiFe_2O_4$ composite as a catalyst followed the Langmuir-Hinshelwood method [45]. The reaction rate constant was determined using the Langmuir-Hinshelwood equation;

$$ln\ (Co/C) = k\ t$$

where k is the reaction rate constant (minute^{-1}), Co is the initial concentration of the solution, and C is the concentration at time t. As seen in Fig. 7c, it can be concluded that the photocatalytic reaction for both the degradation of Rhodamine B and Methylene Blue was first order based on the optimum R^2 values of 0.9857 and 0.9775, in which the k value is linearly dependent on the concentration of only one reactant [28]. The reaction rate constants (k) obtained from the calculation were 0.0162/min for Rhodamine B and 0.0134/min for Methylene Blue. These values were comparable to the value of 0.0096/min for Rhodamine B and 0.0104/min Methylene Blue reported by Neelgund et al. for the pristine ZnO [25] and the value of 0.0062/min found by Naeini et al. for ferrite sample [46]. It is noted that k can be enhanced by combining two phases in a composite sample.

The reaction mechanism of the photocatalysis of dye or any other organic matter can be explained as follows; when the ZnO/$NiFe_2O_4$ composite is exposed to light, the electrons in the valence band of ZnO are excited to the conduction band. They react with oxygen in the liquid forming $O_2^{-\bullet}$. The hydrogen ion formed from the dissociation of a water molecule reacts with O_2^- to form $^\bullet$OH radicals. The $^\bullet$OH radicals are responsible for the degradation of the dye in water [13,28]. The more $^\bullet$OH radicals formed, the faster the photocatalysis proceeds [11]. On the other hand, the photogenerated hole transfer takes place from the valence band of ZnO to the valence band of $NiFe_2O_4$. This suggests that the photogenerated electrons and holes in the heterojunction were efficiently separated.

$$Rd/MB_{(aq)} + NiFe_2O_4/ZnO \rightarrow Rd/MB\text{-}NiFe_2O_4/ZnO \quad (1)$$

$$Rd/MB\text{-}NiFe_2O_4/ZnO + h\nu \rightarrow Rd/MB\text{-}NiFe_2O_4(h^+ + e^-)/ZnO(h^+ + e^-) \quad (2)$$

$$Rd/MB\text{-}NiFe_2O_4(h^+ + e^-)/ZnO + (h^+ + e^-) \rightarrow Rd/MB\text{-}NiFe_2O_4(h^+)/ZnO(e^-) \quad (3)$$

$$e^- + O_2 \rightarrow O_2^{\bullet-} \quad (4)$$

$$O_2 + H^+ + e^- \rightarrow {}^\bullet OH + OH^- \quad (5)$$

$$h^+ + H_2O \rightarrow \bullet OH + H^+ \quad (6)$$

$$Rd/MB\text{-}NiFe_2O_4/ZnO + h^+/\bullet OH/O_2 \rightarrow NiFe_2O_4/ZnO + CO_2 + H_2O + \text{by products} \quad (7)$$

4. Conclusion

In this work, the ZnO/$NiFe_2O_4$ nanocomposite was synthesized via a simple hydrothermal method. The XRD patterns confirmed the formation of both phases. The nanocomposite exhibited spheric and square-like grains when observed using SEM and TEM. The photocatalytic test demonstrated that the ZnO/$NiFe_2O_4$ nanocomposites exhibited high photocatalytic activity on simultaneous degradation of Rhodamine B and Methylene Blue mix solutions, attaining a degradation percentage of ~98% after 3 h of irradiation under the natural sunlight. Photocatalyst performance in mixed solutions showed results that are comparable to the degradation process in each solution. The photodegradation of Rhodamine B and Methylene Blue followed the first order kinetics. In addition, the soft ferromagnetic properties of the nanocomposites allowed for facile separation from a liquid mixture through the application of an external magnetic field, thereby obliviating the need for a solvent extraction step in the process and contributing towards a greener industry with less polluting waste.

Acknowledgments

The authors would like to acknowledge the financial support by LPPM of Andalas University for this work through the KRPGB grant with contract number: SP DIPA 023.017.2.677513/2020.

Conflict-of-Interest Statement

The authors declare that they have no conflict of interest

Author Contributions

Y.S (Associate Professor) conducted the experiments and wrote the original manuscript. T.P.W (Assistant Professor) conducted the experiments and visualized the data. Z. (Associate Professor) provided literature resources and analysis. Z. (Professor) provided valuable research insights and revised the manuscript. R. (Professor) developed the conceptualization, methodology and revised the manuscript.

References

1. Ramachandra M, Pai SDKR, Jaleel JR, Pinheiro D. Improved Photocatalytic Activity of g-C_3N_4/ZnO: A PotentialDirect Z-Scheme Nanocomposite. *ChemistrySelect*. 2020;5:11986-11995. https://doi.org/10.1002/slct.202003166.
2. Dehghani M, Ahmadi B, Zonnoon Y, Nourozi E, Shamsedini N. Decolorization of Direct Red 81 in Aqueous Solutions by Fenton Oxidation Process : Effect of System Parameters. *Iran. J. Heal. Saf. Environ*. 2018;6:1297-1302.
3. Rafiq A, Ikram M, Ali S, Niaz F, Khan M, Khan Q. Maqbool M. Photocatalytic degradation of dyes using semiconductor photocatalysts to clean industrial water pollution. *J. Ind. Eng. Chem.* 2021;97:111-128. https://doi.org/10.1016/j.jiec.2021.02.017.
4. Wang X, Wan X, Xu X, Chen X. Facile fabrication of highly efficient AgI / ZnO heterojunction and its application of methylene blue and rhodamine B solutions degradation under natural sunlight. *Appl. Surf. Sci*. 2014;321:10-18. https://doi.org/10.1016/j.apsusc.2014.09.103.
5. Chamjangali MA, Bagherian G, Javid A, Boroumand S, Farzaneh N. Synthesis of Ag-ZnO with multiple rods (multipods) morphology and its application in the simultaneous photo-catalytic degradation of methyl orange and methylene blue. Spectrochim. *Acta - Part A Mol. Biomol. Spectrosc*. 2015;150:230-237. https://doi.org/10.1016/j.saa.2015.05.067.
6. Huang Y, Wang W, Feng Q, Dong F. Preparation of magnetic clinoptilolite/$CoFe_2O_4$ composites for removal of Sr^{2+} from aqueous solutions: Kinetic, equilibrium, and thermodynamic studies. *J. Saudi Chem. Soc.* 2017;21:58-66. https://doi.org/10.1016/j.jscs.2013.09.005.
7. Al-Kahtani AA. Photocatalytic Degradation of Rhodamine B Dye in Wastewater Using Gelatin/CuS/PVA Nanocomposites under Solar Light Irradiation. *J. Biomater. Nanobiotechnol*. 2017;8:66-82. https://doi.org/10.4236/jbnb.2017.81005.
8. Gadore V, Ahmaruzzaman M. Smart materials for remediation of aqueous environmental contaminants. *J. Environ. Chem. Eng.* 2021;9:106486. https://doi.org/10.1016/j.jece.2021.106486.
9. Alardhi SM, Albayati TM, Alrubaye JM. A hybrid adsorption membrane process for removal of dye from synthetic and actual wastewater. *Chem. Eng. Process. - Process Intensif*. 2020;157:108113. https://doi.org/10.1016/j.cep.2020.108113.
10. Kadhum ST, Alkindi GY, Albayati TM. Remediation of phenolic wastewater implementing nano zerovalent iron as a granular third electrode in an electrochemical reactor. *Int. J. Environ. Sci. Technol*. 2022;19:1383-1392. https://doi.org/10.1007/s13762-021-03205-5.
11. Mohammed HA, Hamza A, Adamu IK, Ejila A, Waziri SM, Mustapha SI. BOD 5 removal from tannery wastewater over ZnO- $ZnFe_2O_4$ composite photocatalyst supported on activated carbon, *J. Chem. Eng. Mater. Sci*. 2013;4:80-86. https://doi.org/10.5897/JCEMS2013.0165.
12. Xu J, Zhang T, Qian J, Zhang J. Efficient photocatalysis and sustainable degradation of methylene blue by titanium dioxide and zinc oxide supported on spent FCC catalyst. *J. Mater. Sci. Mater. Electron*. 2021;32:21869-21879. https://doi.org/10.1007/s10854-021-06531-z.
13. Thanh TLT, Thi LN, Dinh TT, Van NN. Enhanced Photocatalytic Degradation of Rhodamine B Using C/Fe Co-Doped Titanium Dioxide Coated on Activated Carbon. *J. Chem*. 2019: 2949316. https://doi.org/10.1155/2019/2949316.
14. Marañon-ruiz VF, Romero-toledo R, Arturo O, Alejandro P. Photocatalytic Degradation of Rhodamine B and Methylene

Orange Using TiO_2-ZrO_2 as Nanocomposite. *Catalysts*. 2021;11: 1-20. https://doi.org/10.3390/catal11091035.
15. Vasiljevic ZZ, Dojcinovic MP, Vujancevic JD, Jankovic-Castvan I, Ognjanovic M, Tadic NB, Stojadinovic S, Brankovic GO, Nikolic MV. Photocatalytic degradation of methylene blue under natural sunlight using iron titanate nanoparticles prepared by a modified sol-gel method: Methylene blue degradation with Fe_2TiO_5. *R. Soc. Open Sci*. 2020;7. https://doi.org/10.1098/rsos.200708.
16. Makropoulou T, Kortidis I, Davididou K, Motaung DE, Chatzisymeon E. Photocatalytic facile ZnO nanostructures for the elimination of the antibiotic sulfamethoxazole in water. *J. Water Process Eng*. 2020;36:101299. https://doi.org/10.1016/j.jwpe.2020.101299.
17. Zhu HY, Jiang R, Fu YQ, Li RR, Yao J, Jiang ST. Novel multifunctional $NiFe_2O_4$ /ZnO hybrids for dye removal by adsorption, photocatalysis and magnetic separation. *Appl. Surf. Sci.* 2016; 369:1-10. https://doi.org/10.1016/j.apsusc.2016.02.025.
18. Guan W, Gao X, Ji G, Xing Y, Du C, Liu Z. Fabrication of a magnetic nanocomposite photocatalysts Fe_3O_4@ZIF-67 for degradation of dyes in water under visible light irradiation. *J. Solid State Chem*. 2017;255:150-156. https://doi.org/10.1016/j.jssc.2017.08.012.
19. Lu C, Bao Z, Qin C, Dai L, Zhu A. Facile fabrication of heterostructured cubic-$CuFe_2O_4$/ZnO nanofibers (c-CFZs) with enhanced visible-light photocatalytic activity and magnetic separation. *RSC Adv*. 2016;6:110155-110163. https://doi.org/10.1039/c6ra23970f.
20. Hou Z, Zou X, Pu X, Wang L, Geng Y. Facile synthesis and improved photocatalytic H2 production of ZnO/Zn_2GeO_4 and ZnO/Zn_2GeO_4-Cu composites. *J. Solid State Chem*. 2021;296: 121965. https://doi.org/10.1016/j.jssc.2021.121965.
21. Huy DK, Khai NPD, Loan TT, Chung HM, Thanh NK, Khai VV. Synthesis and Characterization of $NiFe_2O_4$/ZnO core-shell Nanocomposites. *J. Sci. Math*. 2018;34:35-43. https://doi.org/10.25073/2588-1124/vnumap.4297 35.
22. Feng J, Wang Y, Zou L, Li B, He X, Ren Y, Lv Y, Fan Z. Synthesis of magnetic ZnO/$ZnFe_2O_4$ by a microwave combustion method, and its high rate of adsorption of methylene blue. *J. Colloid Interface Sci.* 2015;438:318-322. https://doi.org/10.1016/j.jcis.2014.10.009.
23. Vaish G, Kripal R, Kumar L. EPR and optical studies of pure $MgFe_2O_4$ and ZnO nanoparticles and $MgFe_2O_4$–ZnO nanocomposite. *J. Mater. Sci. Mater. Electron*. 2019;30: 16518-16526. https://doi.org/10.1007/s10854-019-02028-y.
24. Zhu HY, Jiang R, Fu YQ, Li RR, Yao J, Jiang ST. Novel multifunctional $NiFe_2O_4$/ZnO hybrids for dye removal by adsorption, photocatalysis and magnetic separation. *Appl. Surf. Sci.* 2016;369:1-10. https://doi.org/10.1016/j.apsusc.2016.02.025.
25. Guo X, Zhu H, Li Q. Visible-light-driven photocatalytic properties of ZnO/$ZnFe_2O_4$ core/shell nanocable arrays. *Appl. Catal. B Environ.* 2014;160-161:408-414. https://doi.org/10.1016/j.apcatb.2014.05.047.
26. Shifu C, Wei Z, Wei L, Huaye Z, Xiaoling Y. Preparation, characterization and activity evaluation of p-n junction photocatalyst p-$CaFe_2O_4$/n-ZnO. *Chem. Eng. J.* 2009;155:466-473. https://doi.org/10.1016/j.cej.2009.07.009.
27. Wilson A, Mishra SR, Gupta R, Ghosh K. Preparation and photocatalytic properties of hybrid core-shell reusable $CoFe_2O_4$-ZnO nanospheres. *J. Magn. Magn. Mater*. 2012;324:2597-2601. https://doi.org/10.1016/j.jmmm.2012.02.009.
28. Feng X, Guo H, Patel K, Zhou H, Lou X. High performance, recoverable Fe_3O_4-ZnO nanoparticles for enhanced photocatalytic degradation of phenol. *Chem. Eng. J*. 2014;244:327-334. https://doi.org/10.1016/j.cej.2014.01.075.
29. Rahmayeni, Arief S, Jamarun N, Emriadi, Stiadi Y. Magnetically separable ZnO-$MnFe_2O_4$ Nanocomposites Synthesized in Organic-free Media for Dye Degradation Under Natural Sunlight. *Orient. J. Chem*. 2017;33. https://doi.org/10.13005/ojc/330608.
30. Shen W, Zhang L, Zhao B, Du Y, Zhou X. Growth mechanism of octahedral like nickel ferrite crystals prepared by modified hydrothermal method and morphology dependent magnetic performance. *Ceram. Int.* 2018;44:9809-9815. https://doi.org/10.1016/j.ceramint.2018.02.219.
31. Adeleke JT, Theivasanthi T, Thiruppathi M, Swaminathan M, Akomolafe T, Alabi AB. Photocatalytic degradation of methylene blue by ZnO/$NiFe_2O_4$ nanoparticles. *Appl. Surf. Sci*. 2018;455:195-200. https://doi.org/10.1016/j.apsusc.2018.05.184.
32. Dong C, Zheng X, Li J, Guo D, Wu L, Jiang X, Jiang C, Xue D. Enhanced microwave magnetic properties of Ni ferrite doped ZnO. *IEEE Trans. Magn.* 2013;49:4238-4241. https://doi.org/10.1109/TMAG.2013.2245309.
33. Duta A, Visa M. Simultaneous removal of two industrial dyes by adsorption and photocatalysis on a fly-ash-TiO_2 composite. *J. Photochem. Photobiol. A Chem*. 2015;306:21-30. https://doi.org/10.1016/j.jphotochem.2015.03.007.
34. Rahmayeni, Ramadani A, Stiadi Y, Jamarun N, Emriadi, Arief S. Photocatalytic performance of ZnO-$ZnFe_2O_4$ magnetic nanocomposites on degradation of Congo red dye under solar light irradiation. *J. Mater. Environ. Sci*. 2017;8:1634-1643. http://www.jmaterenvironsci.com/.
35. Hunter BA. Rietica - a visual Rietveld program, Australian Nuclear Science and Technology Organisation. Australia. 2000.
36. Rahmayeni, Putri J, Stiadi Y, Zilfa, Zulhadjri. Green synthesis of $NiFe_2O_4$ spinel ferrites magnetic in the presence of Hibiscus rosa-sinensis leaves extract: Morphology, structure and activity. *Rasayan J. Chem*. 2019;12:1942-1949. https://doi.org/10.31788/RJC.2019.1245304.
37. Cahyana AH, Liandi AR, Yulizar Y, Romdoni Y, Wendari TP. Green synthesis of $CuFe_2O_4$ nanoparticles mediated by Morus alba L. leaf extract: Crystal structure, grain morphology, particle size, magnetic and catalytic properties in Mannich reaction. *Ceram. Int*. 2021;47: 21373-21380. https://doi.org/10.1016/j.ceramint.2021.04.146.
38. Reddy MP, Madhuri W, Sadhana K, Kim IG, Hui KN, Hui KS, Kumar KVS, Reddy RR. Microwave sintering of nickel ferrite nanoparticles processed via sol-gel method. *J. Sol-Gel Sci. Technol*. 2014;70:400-404. https://doi.org/10.1007/s10971-014-3295-7.
39. Judith JV, Vasudevan N. Synthesis of nanomaterial from industrial waste and its application in environmental pollutant remediation. *Environ. Eng. Res.* 2021;27: 200672. https://doi.org/10.4491/eer.2020.672.
40. Rahmayeni, Alfina A, Stiadi Y, Lee HJ, Zulhadjri. Green syn-

thesis and Characterization of ZnO-$CoFe_2O_4$ Semiconductor Photocatalysts Prepared Using Rambutan (Nephelium lappaceum L.) Peel Extract. *Mater. Res.* 2019;22:e20190228 https://doi.org/10.1590/1980-5373-MR-2019-0228.

41. Ren A, Liu C, Hong Y, Shi W, Lin S, Li P. Enhanced visible-light-driven photocatalytic activity for antibiotic degradation using magnetic $NiFe_2O_4/Bi_2O_3$ heterostructures. *Chem. Eng. J.* 2014;258:301-308. https://doi.org/10.1016/j.cej.2014.07.071.
42. He Z, Xia Y, Su J, Tang B. Fabrication of magnetically separable $NiFe_2O_4/Bi_{24}O_{31}Br_{10}$ nanocomposites and excellent photocatalytic performance under visible light irradiation. *Opt. Mater.* 2019;88:195-203. https://doi.org/10.1016/j.optmat.2018.11.025.
43. Sharma HK, Archana R, Ganesh RS, Singh BP, Ponnusamy S, Hayakawa Y, Muthamizhchelvan C, Raji P, Kim DY, Sharma, SK. Substitution of Al^{3+} to Zn^{2+} sites of ZnO enhanced the photocatalytic degradation of methylene blue under irradiation of visible light. *Solid State Sci.* 2019;94:45-53. https://doi.org/10.1016/j.solidstatesciences.2019.05.011.
44. Rachna K, Agarwal A, Singh NB. Preparation and characterization of zinc ferrite—Polyaniline nanocomposite for removal of rhodamine B dye from aqueous solution, *Environ. Nanotechnology. Monit. Manag.* 2018;9:154-163. https://doi.org/10.1016/j.enmm.2018.03.001.
45. Neelgund GM, Oki A. ZnO conjugated graphene: An efficient sunlight driven photocatalyst for degradation of organic dyes. *Mater. Res. Bull.* 2020;129; 110911. https://doi.org/10.1016/j.materresbull.2020.110911.
46. Aghabeikzadeh-Naeini E, Movahedi M, Rasouli N, Sadegh Z. Synthesis of $ZnFe_2O_4$ nanoparticles in presence and absence of Tween-20: Optical property, adsorption and photocatalytic activity. *Mater. Sci. Semicond. Process.* 2018;73:72-77. https://doi.org/10.1016/j.mssp.2017.09.024.